Journal of Biomedical Optics

BiomedicalOptics.SPIEDigitalLibrary.org

Topography and refractometry of sperm cells using spatial light interference microscopy

Lina Liu
Mikhail E. Kandel
Marcello Rubessa
Sierra Schreiber
Mathew B. Wheeler
Gabriel Popescu

SPIE.

Lina Liu, Mikhail E. Kandel, Marcello Rubessa, Sierra Schreiber, Mathew B. Wheeler, Gabriel Popescu, "Topography and refractometry of sperm cells using spatial light interference microscopy," *J. Biomed. Opt.* **23**(2), 025003 (2018), doi: 10.1117/1.JBO.23.2.025003.

Topography and refractometry of sperm cells using spatial light interference microscopy

Lina Liu,[a,b] Mikhail E. Kandel,[a] Marcello Rubessa,[c] Sierra Schreiber,[d] Mathew B. Wheeler,[c,d,e] and Gabriel Popescu[a,e,*]

[a]University of Illinois at Urbana-Champaign, Beckman Institute of Advanced Science and Technology, Department of Electrical and Computer Engineering, Quantitative Light Imaging Laboratory, Urbana, Illinois, United States
[b]Fujian Normal University, Key Laboratory of OptoElectronic Science and Technology for Medicine of Ministry of Education, Fujian Provincial Key Laboratory of Photonics Technology, Fuzhou, Fujian, China
[c]University of Illinois at Urbana-Champaign, Carl R. Woses Institute for Genomic Biology, Urbana, Illinois, United States
[d]University of Illinois at Urbana-Champaign, Department of Animal Science, Urbana, Illinois, United States
[e]University of Illinois at Urbana-Champaign, Department of Bioengineering, Urbana, Illinois, United States

Abstract. Characterization of spermatozoon viability is a common test in treating infertility. Recently, it has been shown that label-free, phase-sensitive imaging can provide a valuable alternative for this type of assay. We employ spatial light interference microscopy (SLIM) to perform high-accuracy single-cell phase imaging and decouple the average thickness and refractive index information for the population. This procedure was enabled by quantitative-phase imaging cells on media of two different refractive indices and using a numerical tool to remove the curvature from the cell tails. This way, we achieved ensemble averaging of topography and refractometry of 100 cells in each of the two groups. The results show that the thickness profile of the cell tail goes down to 150 nm and the refractive index can reach values of 1.6 close to the head. [DOI: 10.1117/1.JBO.23.2.025003]

Keywords: spatial light interference microscopy; topography; refractometry; sperm cell; refractive index.

Paper 170742R received Nov. 18, 2017; accepted for publication Jan. 23, 2018; published online Feb. 27, 2018.

1 Introduction

Assisted reproduction is one of the major methodologies to treat human infertility. Human *in vitro* fertilization (IVF) was first introduced in 1978 to treat some forms of infertility. Currently, in Western societies, up to 4% of all children born are conceived using assisted reproduction technologies (ARTs).[1] The Centers for Disease Control and Prevention report from 2014 shows that 208,768 ART cycles were performed with 57,332 live births.[2] Several studies confirm the "male side" is found to be responsible for 20% to 30% of infertility cases and contribute to 50% cases overall.[3] The factors may be low sperm concentration, poor sperm motility, or abnormal morphology and these can happen singularly or in combination.[4] Other problems are hormone imbalances or blockages in the male reproductive organs. In about 50% of cases, the cause of male infertility cannot be determined.[5] Current research is focused on developing a noninvasive method to evaluate the semen morphology, with the possibility to use the sperm after the evaluation. In this scenario, a method to evaluate the sperm parameters can be a very useful tool to increase the birthrate success after ARTs.

Here, we show that spatial light interference microscopy (SLIM),[6–8] a highly sensitive quantitative-phase imaging (QPI) method, can be used to study unlabeled sperm cells in great detail. QPI is an emerging method that provides quantitative information about transparent specimens, with nanoscale sensitivity and in label-free mode.[9] Various implementations of QPI have been used recently to study the topography of gametes, assuming a certain refractive index.[10–16] Rappaz et al.[17] reported an experimental procedure to calculate both the refractive index and the cellular thickness from the phase shift using digital holographic microscopy. The method relied on imaging the same cell in two solutions of different refractive index. Here, we decouple the "average" thickness and refractive index of a population of sperm cells using high-accuracy QPI of single cells. The results for topography and refractometry of the tail are in the expected range, as revealed by electron microscopy.[18] Remarkably, we found that the refractive index of the cell midpiece (neck) is very high. It is known that this region is mitochondria-rich, which may explain this interesting finding.[19]

2 Materials and Methods

2.1 *Sperm Cell Preparation*

Straws of frozen bovine semen from bulls, previously tested for IVF, were thawed at 37°C for 40 s. The sample was selected by centrifugation (25 min at 300g) on a discontinuous gradient (45% to 80% in Tyrode's modified medium without glucose and albumin). The pellet was reconstituted into 2 ml of IVF medium and centrifuged twice, at 160g and 108g for 10 min. For each sample, pellet was diluted with IVF medium at the concentration of 1×10^6 sperm/ml.[20] The final sample was divided into sample of dry sperm and sample in phosphate-buffered saline (PBS).

2.1.1 *Dry samples*

Ten μl of selected sperm were smeared onto a clean microscope glass slide (24 to 50 mm), left to dry for 10 min, and finally fixed in 98% ethanol for 10 min.[21] Slides were stored at 4°C until the day of the evaluation.

*Address all correspondence to: Gabriel Popescu, E-mail: gpopescu@illinois.edu

1083-3668/2018/$25.00

2.1.2 *Sample in suspension*

Ten μl were mixed with 50 μl of PBS and smeared onto a clean microscope glass slide. To avoid the liquid evaporation, samples were overlaid with a cover slide and sealed with nail polish. Slides were stored at 4°C until the day of the evaluation.

2.2 *Image Processing*

The quantitative-phase image of sperm cells was retrieved from the recorded four intensity images corresponding to 0, $\pi/2$, π, and $3\pi/2$ phase shift. The retrieved method can be found in previous reports.[9] The irradiance distribution at each point $\mathbf{r} = (x, y)$ in the image plane is a function of the phase shift, namely

$$I(\mathbf{r}, \Delta\varphi) = |U_0|^2 + |U_1(\mathbf{r})|^2 + 2|U_0||U_1(\mathbf{r})|\cos[\Delta\phi(\mathbf{r}) + \delta], \quad (1)$$

where $U_1(\mathbf{r})$ is the scattered light from the sample, U_0 is the incident light, and δ is the phase shift introduced by the spatial light modulation (SLM). With the spatially varying phase shift, $\Delta\phi(\mathbf{r})$ can be reconstructed as

$$\Delta\phi(\mathbf{r}) = \arg\left[\frac{I(\mathbf{r}, 3\pi/2) - I(\mathbf{r}, \pi/2)}{I(\mathbf{r}, \pi) - I(\mathbf{r}, 0)}\right]. \quad (2)$$

Then, the phase associated with the image field can be determined as[22]

$$\phi(\mathbf{r}) = \arg\left\{\frac{\frac{|U_1(\mathbf{r})|}{|U_0|}\sin[\Delta\phi(\mathbf{r})]}{1 + \frac{|U_1(\mathbf{r})|}{|U_0|}\cos[\Delta\phi(\mathbf{r})]}\right\}. \quad (3)$$

To obtain the thickness and refractive index, each sperm cell was chosen as the region of interest (ROI) from the quantitative-phase image. For each group, the 100 ROIs were chosen and tiled into a mosaic using ImageJ. Then halo effect due to phase contrast illumination was removed for each selected ROI using a recent procedure developed in our laboratory.[23]

The halo removed ROIs were then further processed using ImageJ. First, the 30-pixel-wide segmented line selection width was carried out to select the sperm neck and tail. Second, the straighten plugin was applied to each new ROI to digitally remove the tail curvature. The 30-pixel values of each cross section along the straight line were retrieved and the profile along each tail was plotted.

3 Results

In this paper, we measure, for the first time to our knowledge, both the topography and refractometer of sperm cells, in a spatially resolved manner. We use a highly sensitive QPI instrument, CellVista SLIM Pro (Phi Optics, Inc.), which is described in Fig. 1(a). The SLIM module[24] attaches to an existing phase contrast microscope and modulates the phase shift of the incident versus scattered light in increments of $\pi/2$. To achieve this precise modulation, the objective pupil plane is relayed at the plane of a phase only SLM. Without modulation on the SLM, we record a common phase contrast image. However, once a phase shift is applied on a mask that matches the ring of the objective ring, a different intensity image is obtained at the camera. Recording four intensity images corresponding to the 0, $\pi/2$, π, and $3\pi/2$ [Fig. 1(b)] phase shift, the phase map

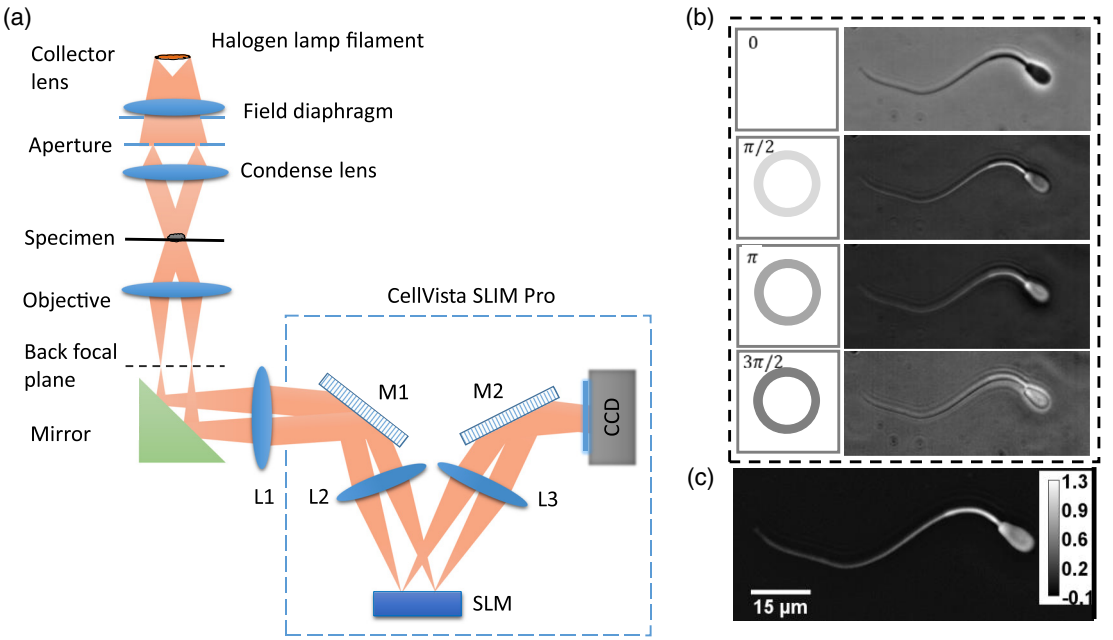

Fig. 1 (a) Schematics of the SLIM. SLIM combines conventional phase contrast microscopy and an SLIM module (Cell Vista SLIM Pro, Phi Optics, Inc.). The SLIM module consists of a 4*f* lens system and an SLM, which produces phase modulation. (b) The phase rings and four intensity images corresponding to 0, $\pi/2$, π, and $3\pi/2$ phase shift recorded by the CCD. (c) High-contrast SLIM quantitative-phase image created by combining the four intensity images. The color bar indicates phase in radian.

associated with the image field can be retrieved quantitatively and uniquely [Fig. 1(c)].

To decouple the cell thickness and refractive index from the optical path length information, we image the cells in two different media: air ($n_0 = 1$) and PBS solution ($n_1 = 1.334$). The cells were prepared as detailed in Sec. 2. We imaged 100 cells for each of the air and PBS groups. As shown in Figs. 2 and 3, we notice immediately that the cell-induced phase shift is significantly lower in PBS versus air, as expected for a smaller refractive index contrast. The spatial path length noise, evaluated as the standard deviation of a background area, shown by the green boxes in Figs. 2(b) and 3(b) is of the order of 1 nm in both cases (see the histograms insets). Note that this noise includes also irregularities in the background due to sample preparation, e.g., debris, solution inhomogeneity, etc. Without a sample, the optical path length noise level achieved by SLIM is below 1 nm.[6]

Each SLIM image provides morphological details that allow us to identify the hallmarks of the cell components [Fig. 4(a)]. Interestingly, the nucleus of the cell appears to have a lower refractive index than the rest of the cell head, which seems to confirm the recent findings on eukaryotic cells.[25,26] To perform averages across different cells, without artifacts due to the curvature, the tail of each cell was numerically "straighten" (Fig. 4) using an ImageJ plugin developed by Meijering et al.[27] In essence, using this tool, we converted the two-dimensional

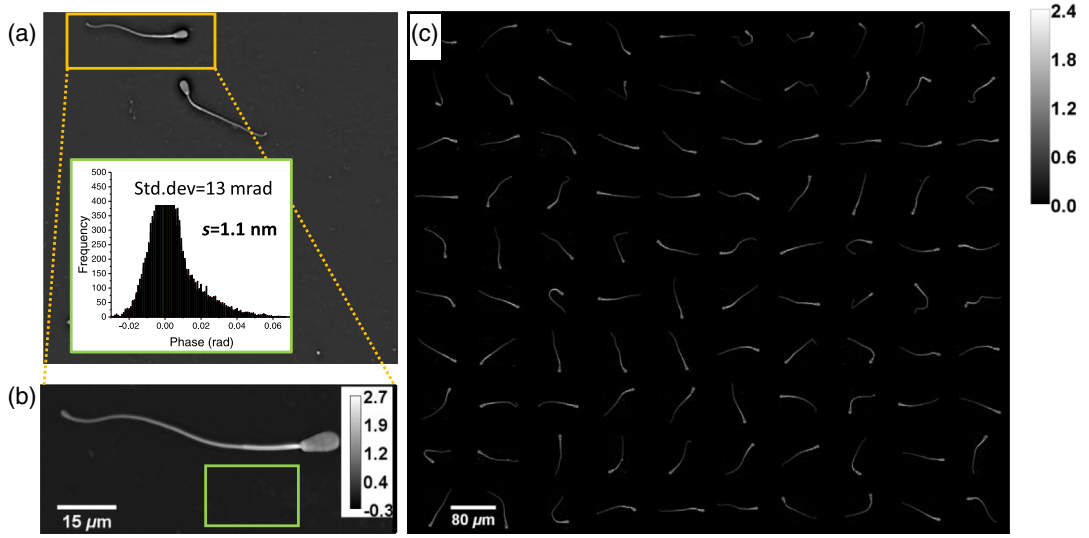

Fig. 2 (a) Example of a single-cell phase image and (b) the corresponding ROI of the "air" group. The standard deviation of a background area marked by the green boxes is shown in the histogram insets. (c) The montage of all the 100 cells measured from this group.

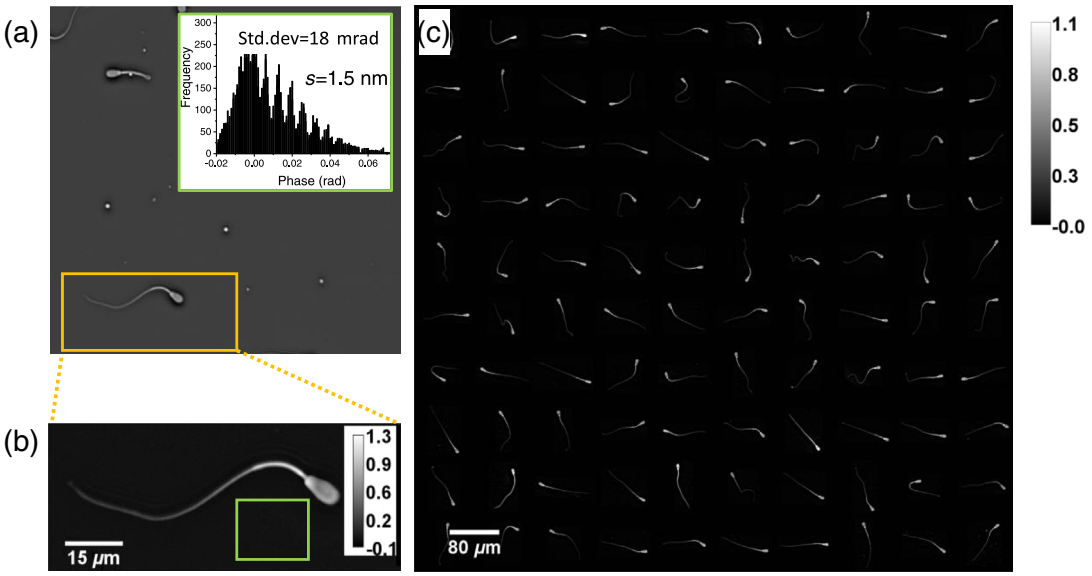

Fig. 3 (a) Example of a single-cell phase image and (b) the corresponding ROI of the "PBS" group. The standard deviation of a background area marked by the green boxes is shown in the histogram insets. (c) The montage of all the 100 cells measured from this group.

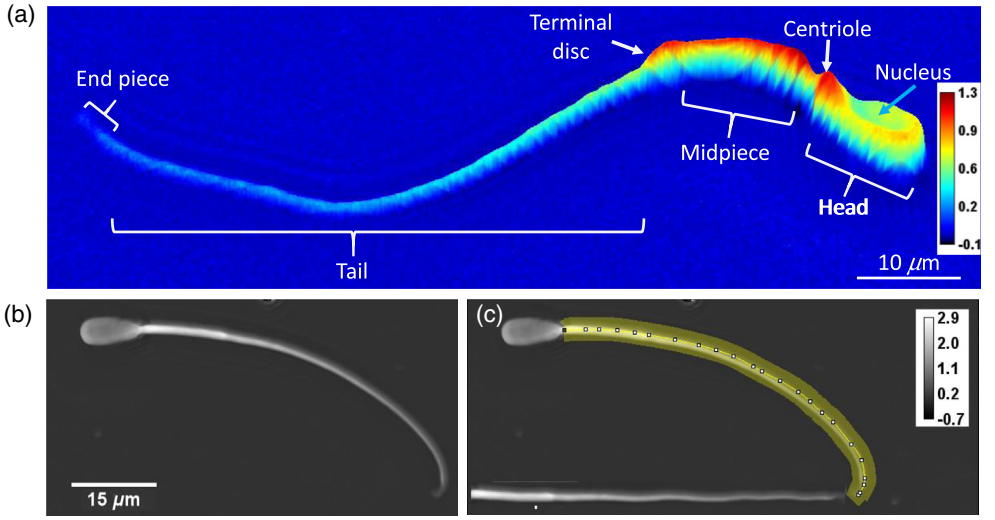

Fig. 4 (a) A sperm cell SLIM image with morphological details and hallmarks of the cellular components (cell in solution). (b) A single sperm with curved tail and (c) the corresponding 30-pixle-wide segmented line along the tail (cell in air). The numerically straighten tail is shown in inset. Color bars in rad.

tail paths into one-dimensional trajectories. Once all tails are converted to lines, we align them such that the point where the neck ends is constant to all of them. With this procedure, we average the phase values of all the cells in each group. To perform the averages over the whole 100-cell set within each group, we only used the length corresponding to the shortest tail in the group. Figure 5 shows the individual phase curves and the resulting two average profiles. The two-phase profiles depend on the average local refractive index, $n(x)$, and thickness $h(x)$, via the following system of equations:[17]

$$\Phi_0(x) = \beta_0[n(x) - n_0]h(x), \tag{4}$$

$$\Phi_1(x) = \beta_0[n(x) - n_1]h(x), \tag{5}$$

where Φ_0 and Φ_1 are the phase shift in air and PBS, respectively, β_0 is the wave number in vacuum $\beta_0 = 2\pi/\lambda$, λ is the wavelength, and x is the coordinate along the tail. Solving the system of equations, we obtain

$$n = (n_1 - 1)\frac{\Phi_1}{\Phi_0 - \Phi_1} + n_1, \tag{6}$$

$$h = \frac{1}{\beta_0}\frac{\Phi_0}{(n-1)}. \tag{7}$$

Note that the two-phase measurements are characterized by a mean, Φ_0 and Φ_1, and standard deviation, $\delta\Phi_0$ and $\delta\Phi_1$, calculated over 100-cell measurements per group. In this way, we perform a statistical average over the cell-to-cell variability in both dry and wet conditions. As a result, the thickness and refractive index profiles are also characterized by standard deviations, δn and δh, which are shown in Fig. 6. The relatively large error bars are due to the variability over the cell population.

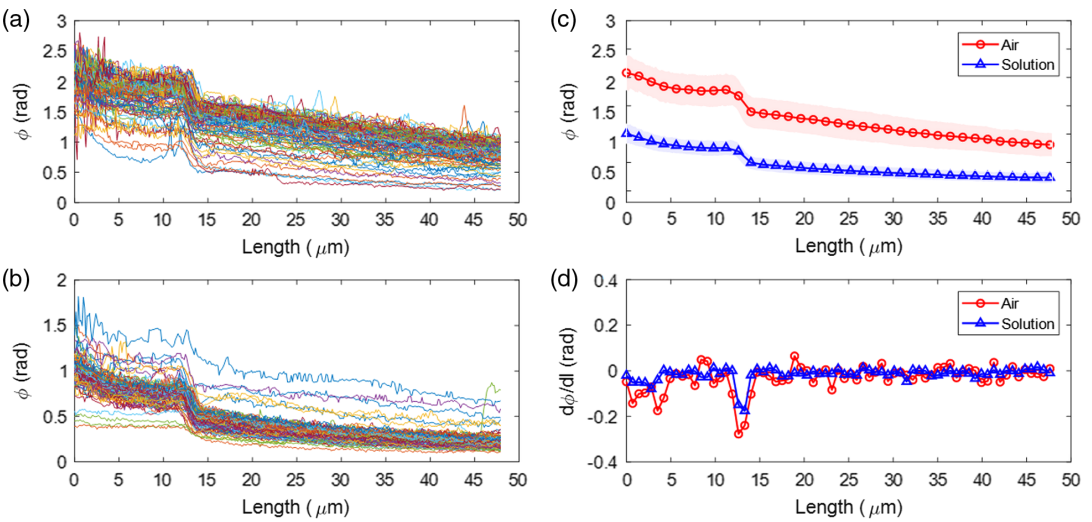

Fig. 5 The individual phase curves of (a) the air group and (b) the PBS group. (c) The resulting two average profiles. (d) First-order derivative of the average profiles, which are used for aligning the thickness and refractive index profiles.

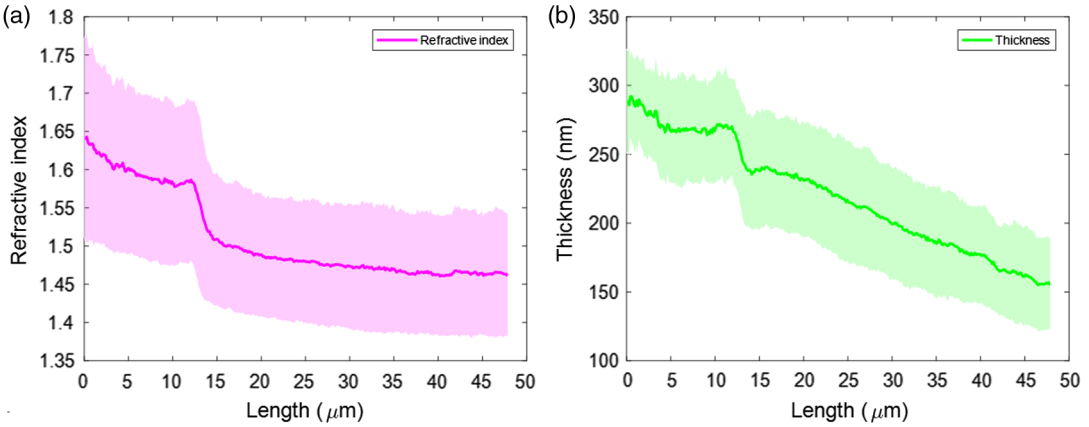

Fig. 6 (a) The refractive index and (b) thickness profiles of spermatozoa. The thickness of the shaded area corresponds to the standard deviation.

The results show that the neck of the sperm is significantly different from the tail not just in terms of thickness but also refractive index. Thus, the thickness decreases along the neck and tail from ~300 to 150 nm. Perhaps the most significant is that the refractive index of the neck reaches very high values, of 1.6 toward the head. The relatively high standard deviations include the intrinsic cell-to-cell variability, since they are the result of averages on two different cell assembles. The values of refractive index decrease toward the tail, down to 1.45, which is comparable to previous reported values. The refractive index of the neck is surprisingly high. It is well known that this region of the cell is packed with mitochondria.[19] These organelles are surrounded by lipid bilayers, which is likely responsible for such high values of refractive index.

4 Summary and Discussion

In summary, we measured for the first time to our knowledge simultaneous topography and refractometry of sperm cells. We performed imaging of cells suspended in two media of different refractive indices, which allowed us to retrieve separately both the thickness and refractive index of the cell tails. Using SLIM, a label-free method capable of providing nanoscale sensitivity to optical path length, we obtained detailed topography from single spermatozoa. Our technique was enabled by numerically eliminating tail curvatures. This procedure allowed us to average the results over a large number of cells in two measurement groups, characterized by different background refractive indices. Recent advances in SLIM technology allow us today to scan entire microscope slides and multiwell plates in a fully programmable and high-throughput manner.[28] The refractive index has been used before as a reporter for biomedical applications.[29–32] We anticipate that these results will open an area of applications by providing more accurate assays for IVF.

Disclosures

Gabriel Popescu has financial interest in Phi Optics, Inc., a company developing QPI technology for materials and life science applications. The remaining authors declare no competing financial interests.

Acknowledgments

This work was supported by the National Science Foundation (Nos. CBET-0939511 STC, DBI 14-50962 EAGER, and IIP-1353368). For more information visit http://light.ece.illinois.edu.

References

1. A. Nyboe Andersen et al., "Assisted reproductive technology and intrauterine inseminations in Europe, 2005: results generated from European registers by ESHRE," *Hum. Reprod.* **24**(6), 1267–1287 (2009).
2. "ART success rates," 2013, http://www.cdc.gov/art/reports/index.html (1 July 2017).
3. A. Agarwal et al., "A unique view on male infertility around the globe," *Reprod. Biol. Endocrinol.* **13**(1), 37 (2015).
4. N. Kumar and A. K. Singh, "Trends of male factor infertility, an important cause of infertility: a review of literature," *J. Hum. Reprod. Sci.* **8**(4), 191–196 (2015).
5. A. B. Jose-Miller, J. W. Boyden, and K. A. Frey, "Infertility," *Am. Fam. Physician* **75**(6), 849–856 (2007).
6. Z. Wang et al., "Spatial light interference microscopy (SLIM)," *Opt. Express* **19**(2), 1016 (2011).
7. Z. Wang et al., "Spatial light interference tomography (SLIT)," *Opt. Express* **19**(21), 19907–19918 (2011).
8. T. Kim et al., "White-light diffraction tomography of unlabeled live cells," *Nat. Photonics* **8**(3), 256–263 (2014).
9. G. Popescu, "Spatial light interference microscopy (SLIM)," in *Quantitative Phase Imaging of Cells and Tissues*, pp. 226–233, McGraw Hill, New York (2011).
10. G. Caprio et al., "Holographic imaging of unlabelled sperm cells for semen analysis: a review," *J. Biophotonics* **8**(10), 779–789 (2015).
11. G. Di Caprio et al., "Quantitative label-free animal sperm imaging by means of digital holographic microscopy," *IEEE J. Sel. Top. Quantum Electron.* **16**(4), 833–840 (2010).
12. A. De Angelis et al., "Combined Raman spectroscopy and digital holographic microscopy for sperm cell quality analysis," *J. Spectrosc.* **2017**, 9876063 (2017).
13. M. A. Ferrara et al., "Label-free imaging and biochemical characterization of bovine sperm cells," *Biosensors* **5**(2), 141–157 (2015).
14. P. K. Poola et al., "Quantitative label-free sperm imaging by means of transport of intensity," *Proc. SPIE* **9718**, 97180O (2016).
15. S. K. Mirsky et al., "Automated analysis of individual sperm cells using stain-free interferometric phase microscopy and machine learning," *Cytometry* **91**(9), 893–900 (2017).
16. T. H. Nguyen et al., "Gradient light interference microscopy for 3D imaging of unlabeled specimens," *Nat. Commun.* **8**(1), 210 (2017).
17. B. Rappaz et al., "Measurement of the integral refractive index and dynamic cell morphometry of living cells with digital holography," *Opt. Express* **13**(23), 9361–9373 (2005).
18. B. Baccetti et al., "Submicroscopic mathematical evaluation of spermatozoa in assisted reproduction. 4. The bovine fertilization (Notulae seminologicae 10)," *J. Submicrosc. Cytol. Pathol.* **29**(4), 563–582 (1997).

19. R. Saacke and J. Almquist, "Ultrastructure of bovine spermatozoa. II. The neck and tail of normal, ejaculated sperm," *Dev. Dynam.* **115**(1), 163–183 (1964).
20. A. Sattar et al., "The influence of gamete co-incubation length on the in vitro fertility and sex ratio of bovine bulls with different penetration speed," *Reprod. Domest. Anim.* **46**(6), 1090–1097 (2011).
21. R. Raghunathan et al., "Optical coherence tomography for embryonic imaging: a review," *J. Biomed. Opt.* **21**(5), 050902 (2016).
22. Z. Wang and G. Popescu, "Quantitative phase imaging with broadband fields," *Appl. Phys. Lett.* **96**, 051117 (2010).
23. M. Kandel et al., "Real-time halo correction in phase contrast imaging," *Biomed. Opt. Express* **9**(2), 623–635 (2018).
24. P. Cintora et al., "Cell density modulates intracellular mass transport in neural networks," *Cytometry* **91**(5), 503–509 (2017).
25. M. Schürmann et al., "Cell nuclei have lower refractive index and mass density than cytoplasm," *J. Biophotonics* **9**(10), 1068–1076 (2016).
26. W. Choi et al., "Tomographic phase microscopy," *Nat. Methods* **4**(9), 717–719 (2007).
27. E. Meijering et al., "Design and validation of a tool for neurite tracing and analysis in fluorescence microscopy images," *Cytom. Part. A.* **58**(2), 167–176 (2004).
28. M. E. Kandel et al., "Label-free tissue scanner for colorectal cancer screening," *J. Biomed. Opt.* **22**(6), 066016 (2017).
29. H. Ding et al., "Optical properties of tissues quantified by Fourier-transform light scattering" *Opt. Lett.* **34**(9), 1372 (2009).
30. Z. Wang et al., "Topography and refractometry of nanostructures using spatial light interference microscopy," *Opt. Lett.* **35**(2), 208–210 (2010).
31. Z. Wang, H. Ding, and G. Popescu, "Scattering-phase theorem," *Opt. Lett.* **36**(7), 1215 (2011).
32. Z. Wang et al., "Tissue refractive index as marker of disease," *J. Biomed. Opt.* **16**(11), 116017 (2011).

Lina Liu is an associate professor at Fujian Normal University and mainly takes part in the research work on photodiagnosis of cancers and photodynamic therapy for skin disease. She is also interested in the research work on quantitative phase imaging. She was a visiting scholar in Dr. Gabriel Popescu's Group at the Department of Electrical and Computer Engineering (ECE), University of Illinois, Urbana-Champaign (UIUC) from August 2016 to July 2017.

Mikhail E. Kandel is a PhD candidate in electrical and computer engineering at the UIUC. He is working in the Quantitative Light Imaging (QLI) Lab at Beckman Institute of Advanced Science and Technology. He develops computational tools and instrumentation for phase-shifting interferometers. His research interests include studying image formation to improve tomography, time-lapse microscopy to monitor cell populations, and developing new markers to remove observer bias in pathology.

Marcello Rubessa is a research assistant professor in animal sciences at the UIUC. His research interests include embryo biology, regenerative medicine, and stem cells. He has been published 60 times between abstract and journal articles, five conference and technical articles, one book chapter, and has obtained two patents.

Sierra Schreiber is an undergraduate student conducting research in the Department of Animal Sciences at the University of Illinois.

Matthew B. Wheeler is a professor in animal sciences, bioengineering at the College of Medicine at the UIUC. His research interests included embryo biology, regenerative medicine, microfluidics, and gene expression during cell differentiation. He has published 140 journal articles, 55 conference and technical articles, 225 conference abstracts, 39 book chapters, 1 book on biotechnology, and has obtained 23 patents. He has presented 212 invited/keynote/plenary talks.

Gabriel Popescu is a professor in electrical and computer engineering at UIUC. His research is focused on biomedical optics and quantitative phase imaging (QPI) of cells and tissue. He has published a book on QPI, authored 150 journal publications and 200 conference presentations, authored 29 issued and pending patents, and given 185 invited/keynote/plenary talks. He founded Phi Optics, Inc., a startup company that commercializes quantitative phase imaging technology. He is a fellow of OSA and SPIE.